This is a preprint, the final version is subject to change, of the American Mineralogist (MSA)
Cite as Authors (Year) Title. American Mineralogist, in press.
DOI: https://doi.org/10.2138/am-2019-6797

Revision 1

Energetics of Ethanol and Carbon Dioxide Adsorption on Anatase, Rutile and γ-Alumina Nanoparticles

Lili Wu[1], Xin Guo[1], and Alexandra Navrotsky[1,*]

[1]Peter A. Rock Thermochemistry Laboratory and NEAT ORU, University of California Davis, Davis CA 95616

Abstract

Nanoparticles are widely present in the natural environment. Their surface reactivity, redox ability and adsorption properties are related to geochemical processes. To explore the thermodynamics of interaction between nano oxides and small gas molecules, we applied gas adsorption calorimetry to investigate the energetics of ethanol and carbon dioxide adsorbed on surfaces of nanoscale anatase, rutile and γ-alumina particles. The measured zero-coverage adsorption enthalpies per mole of gas adsorbed are -97.7, -107.3, and -84.8 kJ/mol for C_2H_5OH on anatase, rutile and γ-Al_2O_3, respectively. The corresponding values for CO_2 adsorption are -59.4, -47.4 and -47.1 kJ/mol. The results indicate the ethanol adsorption is generally more exothermic than carbon dioxide and water adsorption. The isotherm and differential enthalpies shows type II isotherms and step-wise patterns for ethanol adsorption in all three oxides. However, CO_2 adsorption shows simple continuous isotherms and energetics which suggest dominant physical adsorption occurred. The repeated adsorption cycle shows that ethanol adsorption on these nanoparticles is partially reversible at room temperature. This thermodynamic evidence indicates that ethanol and similar organics may protect mineral oxide surfaces from reaction with aqueous solutions, which may affect crystal growth, dissolution, and biomineralization.

Introduction

Fine-grained (nanophase) minerals can be produced in the natural environment by rapid precipitation, microbial action, or weathering (Strambeanu *et al,* 2015; Griffin *et al.*, 2018). Many geochemical reactions occur at mineral surfaces in atmospheric, aqueous or hydrothermal environments (Schindler and Hochella, 2015; Hazen *et al.*, 2008). These reactions largely influence chemistry and physical conditions of the atmosphere, ocean, land surface and climate. The transport of nutrients and pollutants is also mediated by surface adsorption and transport by nanoparticles. With unique surface properties and reactivity, nanomaterials have technological

applications as energy storage devices, catalysts, and dielectrics (Farfan-Arribas and Madix, 2002). Binary and ternary metal oxides have been studied extensively, with emphasis on synthesis, crystal structure, surface topography, as well as chemical and physical properties (Paramasivam *et al.,* 2012; Kuang *et al.*, 2008; Köppen *et al.,* 2008).

However, we know relatively little about the thermodynamics of interaction of nanoparticles with target species, such as small organic molecules from experimental measurement. Experimental thermodynamic data are essential to clarify the complex behavior of adsorption in nanoparticles. Adsorption is the physical basis for further chemical or physical processes. It can modulate reactions of various gases on solid surfaces. *In situ* gas adsorption with simultaneous calorimetric measurements to probe water interactions on oxide surfaces has become an important thermodynamic methodology (Ushakov *et al.*, 2005). It has been applied to examine other gases (CO_2, ethanol and methane) adsorption phenomena and associated enthalpies (Lazzeri *et al.*, 2001; Levchenko *et al.,* 2006; Wu *et al.*, 2015). Previous calorimetric studies of water adsorption on nanophase oxides SiO_2, TiO_2, and Al_2O_3 show 60 - 80 kJ/mol of excess hydration energy relative to water vapor condensation (Wu *et al*., 2015; Guo *et al*., 2018), and porous materials such as zeolites and metal organic frameworks possess higher abilities to absorb water (Wu *et al*., 2013). CO_2 molecules favor to bind to hydroxide materials such as layered double hydroxides or metal organic frameworks with adsorption enthalpies of 60 - 110 kJ/mol in magnitude (Radha *et al*., 2014; Wu and Navrotsky, 2013).

Ethanol (C_2H_5OH), having a hydrophobic and a hydrophilic end, is a simple model for organic molecules with higher structural complexity widely present in biological and technological systems. Ethanol - mineral interaction is favorable and sometimes even stronger than that with water since the oxygen has higher charge density than water and can easily attack the metal atoms. By competing with water, ethanol and other organic molecules may stabilize the surface of minerals and retard their dissolution and weathering (Davis and Hayes, 1987). On the other hand, strong interactions on mineral surfaces may weaken and break the intra-molecular bonding of organic molecules and cause dissociative reactions. This is also a natural process (Mattos *et al*., 2012) which has been utilized in photocatalytic for solar energy and to synthesize other molecules (Gupta and Tripathi, 2011).

Molecular and dissociative adsorption represents two contrasting binding mechanisms of ethanol on metal oxides (Muir *et al.,* 2012). Molecular adsorption builds a new surface - ethanol bond without breaking any bonds in the C_2H_5OH molecule, but for dissociative adsorption, surface - ethanol bond formation is accompanied by the deprotonation of ethanol and the bonding of that proton directly to a surface oxygen species

to form an OH species. A TPD/MS study of ethanol adsorption on TiO_2 (110) surfaces showed that heating results in recombination of about 50 % of the dissociative adsorption sites by overcoming a moderate kinetic barrier (Farfan-Arribas and Madix, 2002). In contrast, an STM study suggested that ethanol adsorbed on TiO_2 (001) is mobile and adsorption is reversible, even at relatively low temperatures, which implies a small kinetic barrier (Leon *et al.*, 2013). However, the dissociative adsorption process is associated with a relatively high kinetic barrier. Thus the ethanol adsorption - desorption process is complex kinetically and may be complex thermodynamically as well.

CO_2 is one of the critical components in mineral evolution and bio-organic lifecycles. There is great interest in the study of CO_2 adsorption in relation to carbon sequestration, the carbon cycle, and new energy resources (Batjes, 1998; Amouroux *et al.*, 2014). Previous research has suggested generally weak CO_2 adsorption on oxide surfaces, due to the poor electron donor nature of the oxygen atoms resulting from a strong delocalization effect (Stangeland *et al.*, 2017; Silaghi *et al.*, 2016). At ambient temperature, molecular adsorption happens with one of its oxygen atoms coordinating with a metal atom. Some carbonate species are also observed on anhydrous surfaces (Yahya *et al.*, 2016). Hydration assists CO_2 adsorption by promoting bicarbonate formation. Consistent with its weak adsorption, CO_2 exhibits good mobility and reversibility on metal oxide surfaces.

Many spectroscopic and imaging approaches (including STM, ATR-FTIR, XPS, TPD and MS) (Belhadj *et al.*, 2017; Hwang *et al.*, 1999; Coronado *et al.,* 2003) and computational simulations (Sumita *et al.*, 2010; Zhang *et al.,* 2015; de Armas *et al.*, 2007) have been applied to explain the thermodynamics and kinetics of adsorption and desorption, including the binding site locations, binding patterns and defect effects. Generally, higher energy sites or crystal facets are preferred for initial binding. In particular, there is a higher affinity on defect sites. Computational simulations produce a wide range of predictions for the ethanol adsorption energy on rutile TiO_2 (110), from -69 to -202. kJ/mol on Ti^{4+}(5f) sites, from -141 to -219 kJ/mol at oxygen vacancy sites; and for anatase TiO_2 (101), from -111 to -119 kJ/mol on Ti^{4+}(5f) sites, -169 kJ/mol on Ti^{4+}(5f) next to oxygen vacancies, and -419 kJ/mol at oxygen vacancy sites (Sumita *et al.*, 2010; Zhang *et al.*, 2015; de Armas *et al*,. 2007). Due to the complexity of solid surfaces, especially for these nanoparticles, which display more coordination desaturation, point defect formation, and synthesis dependent exposure of facets than the idealized surfaces used in computational studies, the systematic energetic map along all of these surface states is not easy to clarify without experimental validation.

In this study, we report the first calorimetric data for ethanol and carbon dioxide adsorption on the surface of nanoscale TiO_2(7 nm anatase and 20 nm rutile) and 30 nm γ-Al_2O_3. (particle size determined from BET surface area and confirmed by XRD, see below) The adsorption isotherm and associated differential heat effect have been measured. The results show distinct adsorption patterns for different oxides with different gases. The variation in binding energy with coverage has been monitored by mapping the adsorption differential enthalpy. The data are discussed and compared with earlier studies of ethanol and carbon dioxide adsorption on silica and of water adsorption on a variety of oxides.

Experimental Methods

The nano rutile $TiO_2$was synthesized by Li (Li, *et al*., 2003) through a hydrothermal method. Nano anatase TiO_2 was from Levchenko's synthesis (Levchenko *et al.,* 2006) using a modified sol-gel method. γ-alumina was synthesized by using an aqueous co-precipitation method which does not involve any organics or polymeric precursors (Rufner *et al*., 2013).

Thermogravimetric analysis and differential scanning calorimetry (TG-DSC) were performed on all samples using a Setaram Labsys instrument. Samples were heated from 25 to 1000 °C at 10 °C/min under dry air. Powder X-ray diffraction patterns (PXRD) were obtained using a Bruker AXS D8 Advance diffractometer operated with Cu Ka radiation (λ=1.54 Å). The data were collected in the 2θ range of 10 to 70°, with a step size of 0.02° and dwell time of 1 s per step. The XRD pattern analysis was conducted for phase identification and crystal size by Jade 6.5. Rietveld refinement was applied for data analysis. Crystal size estimation was based on the Scherrer equation and Williamson-Hall plot (Scherrer, 1918; Williamson and Hall, 1953). A number of well resolved peaks were fitted and the observed peak shapes can be represented with a pseudo-Voigt function, a simple approximation to the convolution of Gaussian and Lorentzian functions. The Gaussian and Lorentzian half widths, G and L, representing the effect of instrumental resolution(V) and particle-size(X) broadening respectively, which with Bragg angle θ can be derived from the functions V$\tan\theta$ and X/$\cos\theta$. The XRD patterns are shown in Figure 1.

The surface areas were measured by N_2 adsorption and calculated based on the BET equation (Brunauer *et al*., 1938). The particle sizes were calculated based on the hypothesis of spherical particles by using the density (ρ) and measured surface area (SA).

TiO_2 and γ-Al_2O_3 nano particles before and after ethanol and CO_2 adsorption were further characterized by Raman spectroscopy. The Raman spectra were obtained with a Renishaw RM1000 system integrated with Leica DMLM microscope and a motorized stage using an argon ion laser (514.5 nm) operating at 9 A and 20 mW. The Raman signal was collected in a static range 1000–100 cm^{-1} with 10 accumulations of 40 s each. A standard silicon film was used to calibrate Raman shifts.

The enthalpies of ethanol and CO_2 adsorption were measured by a gas adsorption calorimetry system, which includes a Calvet-type microcalorimeter (Setaram Sensys) coupled to a gas adsorption analyzer (Micromeritics ASAP 2020), as described previously (Ushakov, 2005). According to the surface area of each sample, powder weights of 20 - 50 mg were used and carefully transferred to one side of a forked tube, the other side left empty as a reference for the calorimetric measurement. The samples were heated (degassed) at 200 °C under vacuum for 2 h before the adsorption experiment. The temperature and time were chosen in prior experiments to remove the surface water without coarsening the samples. This procedure was done in the same forked tube used for adsorption calorimetry and the samples were not exposed to any atmosphere between degassing and calorimetry. Doses of 1-5 μmol of CO_2 or ethanol were introduced to the sample tube and the pressure change was monitored. This produced the isotherm during the experiment. Each dose of gas gave a heat signal peak corresponding to the surface interaction with gas molecules. A typical calorimetry trace for ethanol adsorption on rutile TiO_2 is shown in Figure 2.

Results and Discussion

Characterization

The TG-DSC results are shown in Figure 3. Both anatase and rutile TiO_2 show a first endothermic peak and weight loss at around 100 °C and γ-alumina shows similar dehydration behavior at 150 °C. The broad exothermic peaks at 350, 400 and 370 °C are related to aggregation and coarsening of the three nanophase oxides. Based on these results, a degas temperature of 200 °C for 2 h was applied to remove the surface water before the adsorption experiment. To check the size change, oxides were subjected to XRD (Fig. 1) after degassing. The XRD pattern refinement of anatase, rutile TiO_2 and γ-alumina before and after degassing indicates that crystal growth and phase change did not occur during the degassing operation. The same degas condition was used for both BET and gas adsorption experiments.

Raman spectra of TiO_2 before and after gas adsorption are shown in Fig 4a and 4b, in which a slight blue shift was observed after the adsorption of CO_2 and ethanol for both rutile and anatase, suggesting some chemical

bond formation. The B_{1g} mode in anatase with ethanol adsorption, caused by the symmetric bending vibration of O-Ti-O, splits into two broad peaks. One is close to the original and the other experiences a large blue shift, which may arise from the dissociative chemical binding of ethanol molecules. Evidence of this dissociative chemical adsorption was later observed is irreversible adsorption. For rutile, only a small blue shift was observed for the B_{1g} vibrational mode. The γ-Al_2O_3 doesn't show Raman spectra but only fluorescent background.

Adsorption isotherms

The isotherms for ethanol adsorption are plotted in Figure 5a, 6a, and 7a for anatase, rutile, and γ-Al_2O_3, respectively. The associated calorimetric traces are plotted with absorbed amounts in Fig 5b, 6b, and 7b. Those for CO_2 adsorption are plotted in Fig 8.

Ethanol adsorption for all three oxides demonstrates type II isotherms, which indicate strong chemisorption. Each isotherm has three stages with two inflection points: In the first stage, the isotherm shows a nearly vertical curve at near-zero coverage at low pressure associated with a large exothermic heat effect. In the second stage, increasing partial pressure and absorbed quantity are associated with less exothermic differential enthalpies. According to the differential enthalpy maps, these patterns must denote gas molecules adsorbing onto and fully loading sites with weaker bonding, followed by just van der Waals interaction, which represents physisorption. The differential enthalpy curve of ethanol adsorption on anatase shows more steps than that of rutile, which signifies that the anatase has a less uniform surface with distinguishable energy states. In the third stage, the isotherm reaches the condensation pressure of ethanol and shows a vertical line which reaches the equilibrium pressure. The corresponding energetic maps show a horizontal line which indicates the condensation of free ethanol. These stepwise patterns of isotherms for nanophase oxides have also been seen in those of ethanol adsorption on nano porous materials (Wu *et al*., 2015).

Adsorption experiments for two of oxides have been repeated up to two times to test the stability of adsorption. After the first run, the samples were subjected to 12 h of evacuation without heating. The second run shows a simple type I isotherm curve. The stepwise behavior of the first two stages is simplified in the second isotherm, as are the enthalpy maps (Fig. 5-7). The inflection point after the physisorption on the isotherm appears at a much lower adsorption amount. The third runs are similar to the second. This behavior indicates that chemisorption and dissociative adsorption are irreversible under mild degas conditions.

In contrast to ethanol adsorption, CO_2 adsorption on the three nanophase oxides shows type II and type III isotherms, which indicate weaker interaction than for ethanol. As shown in Fig. 7, the isotherms of CO_2

adsorption on rutile and γ-Al_2O_3 are typical of type III adsorption. The nearly linear relation between pressure and adsorbed amount denote that CO_2 only has weak interactions on the surface. However, CO_2 adsorption on anatase TiO_2 lacks a clear inflection point, which is between type II and type III isotherms, suggesting that a second adsorption layer may form before the completion of monolayer adsorption.

Enthalpies of adsorption

The values of the first differential enthalpies (approximating zero-coverage adsorption) and integral enthalpies are summarized in Table 1. For ethanol adsorption, the differential enthalpies for the first dose are -97.7 kJ/mol for anatase TiO_2, -107.3 kJ/mol for rutile TiO_2, and -84.8 kJ/mol for γ-Al_2O_3. The integral enthalpies, which represent the overall heat effect caused by surface interactions, are -77.1, -100.6 and -72.5 kJ/mol for anatase, rutile, and γ-Al_2O_3. The value for rutile is more exothermic than that of anatase, agreeing with the smaller surface energy of anatase (Levchenko et al., 2006).

The surface coverages are 2.81, 1.73 and 3.05 molecules of ethanol per nm^2 for anatase, rutile, and γ-Al_2O_3. In the second run, the average apparent surface coverages decrease to 0.64, 0.47 and 1.2 molecules/nm^2, respectively. The surface coverage differences between the first and the second runs represent the irreversible portions of gas adsorption which are 2.17, 1.36 and 1.85 molecules/nm^2. According to the inflection point on the isotherms (first run), the calculated first layer adsorptions are 2.41, 1.56 and 2.66 molecules/nm^2 for the three samples, which are greater than the irreversible amounts in each case. Thus some strongly bound ethanol may in fact be desorbed during the mild degassing, which indicates significant mobility of adsorbed ethanol at ambient conditions. γ-Al_2O_3 has a slightly less exothermic integral enthalpy of ethanol adsorption than anatase, but shows generally similar behavior.

The observed strong and partially irreversible ethanol adsorption suggests that dissociative adsorption has occurred, and the more exothermic zero-coverage enthalpy on rutile than on anatase may be caused in part by oxygen defects on the surface. Some evidence of more defects on rutile is the slight color change from white to grey after degassing at 200 °C. Such color change was not observed on anatase. Grey or even black rutile can be prepared by heating under high vacuum (Sclafani and Herrmann, 1996), which is strong evidence for increasing oxygen vacancy concentration and dramatic decrease of the bandgap. Anatase has a lower tendency for oxygen vacancy generation than rutile (Xu *et al*,. 2011).

The differential enthalpies for CO_2 adsorption of all three oxides are in the range of physisorption. As shown in Table 2, the differential enthalpies of CO_2 adsorption from the first dose (zero-coverage adsorption) are -59.4 kJ/mol for anatase, -47.4 kJ/mol for rutile, and -47.1 kJ/mol for γ-Al_2O_3. The integral enthalpies are -41.6, -39.1 and -33.7 kJ/mol. The integral enthalpies are dramatically less exothermic than those of ethanol and water. The surface coverages are 2.22, 1.19 and 1.92 CO_2/nm^2 for the three samples, which are also smaller than those for ethanol, but in a similar order. The relatively small value of surface coverage might be explained by different types and numbers of binding sites and repulsion among adsorbed CO_2 molecules. Notably, CO_2 adsorption is less exothermic on rutile than on anatase even through rutile has more O-defect sites. The coverage on anatase is higher than that on rutile. This might indicate more sites available for CO_2 on anatase than rutile. Differences in binding sites may also affect the energetics of the second layer of ethanol but there is no direct structural information to identify such differences. Both isotherm and integral enthalpy data indicate that there are only weak interactions between CO_2 and minerals with anhydrous surfaces. This is in contrast to the large uptake and stronger adsorption of CO_2 on layered double hydroxides (LDH) (Radha *et al.*, 2014), for which the hydrous surface, hydroxyl groups, and interlayer sites appear to promote CO_2 adsorption.

Comparison of ethanol and water adsorption

The integral enthalpies of ethanol adsorption are more exothermic than those of water adsorption of anatase (-62 kJ/mol) and rutile (-84 kJ/mol) (Levchenko *et al.,* 2006). However, the integral enthalpy of water adsorption on γ-Al_2O_3 (- 72 kJ/mol) (Castro, *et al*., 2012) is the same as that of ethanol adsorption. Differences in the degree of dissociative adsorption may account for these observations.

The integral enthalpy of CO_2 adsorption on anatase is more exothermic than on rutile and γ-Al_2O_3 which is different than the pattern shown for ethanol adsorption. The reasons for these differences are not clear but different surface sites and differing extents of structuring of the first few layers of the adsorbed molecules may play a role., as suggested previously for ethanol on calcite and silica surfaces (Wu and Navrotsky, 2013, 2015; Wu et al. 2015). The stronger energetics of interaction of TiO_2 with ethanol than water may be meaningful in biogeochemical processes. The mechanism is likely that the ethyl group points away from the oxide surface and creates a somewhat hydrophobic layer separating the surface from the atmosphere or aqueous solution. This means that a mineral surface similar to that of TiO_2 has a large preference to react with organic molecules like ethanol, which has a hydrophilic (hydroxyl) end. Such preferential adsorption will slow aqueous dissolution by making the surface less accessible to water molecules. Furthermore such organic sorbents may facilitate mineral - protein

and mineral - microbe interaction that may be involved in bio-mineralization. However, other oxides, such as γ-Al_2O_3, may behave differently.

Comparison with other materials

Calorimetric studies of ethanol and CO_2 adsorption on other materials (silica, zeolites, calcite, layered double hydroxides and metal organic frameworks) have been reported previously (Wu and Navrotsky, 2013, 2015; Guo, *et al*., 2018; Radha and Navrotsky, 2014). The zero-coverage enthalpies of ethanol adsorption on silica glass (CPG-10, −72.7 kJ/mol) (Wu and Navrotsky, 2015) and crystalline porous zeolitic silica (SSZ-59, -52.5 kJ/mol; MCM-41, -49.1 kJ/mol; and SBA-15, -51.3 kJ/mol) (Wu and Navrotsky, 2013) are less exothermic than those of TiO_2 and γ-Al_2O_3. The reason could be that continuous framework structures of these silica materials provide only few sites capable of dissociative binding.

For CO_2 adsorption, the integral enthalpies on layered double hydroxides (-65.1kJ/mol) (Radha and Navrotsky, 2014) are close to the reaction enthalpy of aqueous hydroxide with gaseous CO_2 to form bicarbonate ($CO_2+OH^- \rightarrow HCO_3^-$) at room temperature, -66 kJ/mol (Sanz-Pérez *et al*., 2016). The adsorption on a metal organic framework CD-MOF-2 (–113.5 kJ/mol) (Wu *et al.,* 2013) are close to the enthalpy of formation of calcite from portlandite ($CO_2+Ca(OH)_2 \rightarrow CaCO_3+H_2O$), -109 kJ/mol (Sanz-Pérez *et al*., 2016). Both these systems, similar to the hydrated alumina surface, have basic hydroxyl groups, which can form bicarbonate or carbonate species with CO_2. The stronger CO_2 binding in those materials supports the idea that hydration is a key factor to evolve the weak binding in anhydrous anatase, rutile, and γ-Al_2O_3, toward stronger CO_2 capture.

Implications

This study provides new thermodynamic evidence and comparison of the behavior of ethanol, water, and carbon dioxide on the surfaces of anatase, rutile, and γ-alumina. Ethanol, representative of a larger class of small organic molecules, binds more strongly than water on both anatase and rutile TiO_2, presumably through its hydrophilic OH end, leaving the ethyl group pointing away from the surface. Such strong binding may protect the surface from further attack by water and provide mechanisms for biological control of mineral synthesis and dissolution. However, γ-Al_2O_3 has very similar energetics for water and ethanol binding and other minerals may behave differently. CO_2 is more weakly adsorbed than water and ethanol on all three dry minerals. Future work should look at the interactions between water and carbon dioxide adsorption, where formation of carbonate and bicarbonate groups may lead to stronger surface interactions.

Acknowledgments

This research was supported by the U.S. Department of Energy, Office of Basic Energy Sciences, grant ER97-14749. We thank Sergey Ushakov for assistance in the gas adsorption experiments and Pardha Saradhi Maram for help with Raman spectroscopy.

References

Amouroux, J., Siffert, P., Pierre Massué, J., Cavadias, S., Trujillo, B., Hashimoto, K., Rutberg, P., Dresvin, S., and Wang, X. (2014) Carbon dioxide: A new material for energy storage. Progress in Natural Science: Materials International, 24(4), 295-304.

Batjes, N. H. (1998). Mitigation of atmospheric CO_2 concentrations by increased carbon sequestration in the soil. Biology and Fertility of Soils, **27**(3), 230-235.

Belhadj, H., AlSalka, Y., Robertson, P., and Bahnemann, D.W. (2017) In Situ ATR-FTIR Investigation of the effects of H_2O and D_2O adsorption on the TiO_2 surface. ECS Transactions, 75(50), 101-113.

Brunauer, S., Emmett, P.H., and Teller, E. (1938) Adsorption of gases in multimolecular layers. Journal of the American Chemical Society, 60(2), 309-319.

Castro, R. H. R. and D. V. Quach (2012) Analysis of anhydrous and hydrated surface snergies of gamma-Al_2O_3 by water adsorption microcalorimetry. The Journal of Physical Chemistry C **116**(46): 24726-24733.

Castro, R.H.R., Ushakov, S.V., Gengembre, L., Gouvêa, D., and Navrotsky, A. (2006) Surface Energy and Thermodynamic stability of γ-alumina: effect of dopants and water. Chemistry of Materials, 18(7), 1867-1872.

Coronado, J.M., Kataoka, S., Tejedor-Tejedor, I., and Anderson, M.A. (2003) Dynamic phenomena during the photocatalytic oxidation of ethanol and acetone over nanocrystalline TiO_2: simultaneous FTIR analysis of gas and surface species. Journal of Catalysis, 219(1), 219-230.

Davis, J.A., and Hayes, K.F. (1987) Geochemical Processes at mineral surfaces: an overview. Geochemical Processes at Mineral Surfaces, 323, p. 2-18. American Chemical Society.

de Armas, R.S., Oviedo, J., San Miguel, M.A., and Sanz, J.F. (2007) Methanol adsorption and dissociation on TiO_2(110) from first principles calculations. The Journal of Physical Chemistry C, 111(27), 10023-10028.

Farfan-Arribas, E. and R. J. Madix (2002) Role of defects in the adsorption of aliphatic alcohols on the TiO_2(110) surface. The Journal of Physical Chemistry B, 106(41), 10680-10692.

Griffin S., Masood M., Nasim M., Sarfraz M., Ebokaiwe A., Schäfer K.-H., Keck C., and Jacob C. (2018) Natural nanoparticles: a particular matter inspired by nature, Antioxidants, 7(1), 3.

Guo, X., Wu, L., and Navrotsky, A. (2018) Thermodynamic evidence of flexibility in H_2O and CO_2 absorption of transition metal ion exchanged zeolite LTA. Physical Chemistry Chemical Physics, 20(6), 3970-3978.

Gupta, S.M., and Tripathi, M. (2011) A review of TiO_2 nanoparticles. Chinese Science Bulletin, 56(16), 1639.

Hazen RM., Papineau D., Bleeker W., Downs RT., Ferry J., McCoy T., Sverjensky D., Yang H. (2008) Mineral evolution, American Mineralogist, 93, 1693-1720.

Hwang, S.-J., and Raftery, D. (1999) In situ solid-state NMR studies of ethanol photocatalysis: characterization of surface sites and their reactivities. Catalysis Today, 49(4), 353-361.

Inel G. A., Ungureau E.-M., Varley T. S., Hirani M., and Holt K. B. (2016) Solvent–surface interactions between nanodiamond and ethanol studied with in situ infrared spectroscopy, Diamond and Related Materials, 61, 7-13.

Köppen S., Bronkalla O., and Langel W. (2008) Adsorption Configurations and energies of amino acids on anatase and rutile surfaces, The Journal of Physical Chemistry C, **112**(35), 13600-06.

Kuang, D., Brillet, J., Chen, P., Takata, M., Uchida, S., Miura, H., Sumioka, K., Zakeeruddin, S.M., and Grätzel, M. (2008) Application of highly ordered TiO_2 nanotube arrays in flexible dye-sensitized solar cells. ACS Nano, 2(6), 1113-1116.

Lazzeri, M., Vittadini, A., and Selloni, A. (2001) Structure and energetics of stoichiometric TiO_2 anatase surfaces. Physical Review B, 63(15), 155409.

Leon, C.P., Sagisaka, K., Fujita, D., and Han, L. (2014) Ethanol adsorption on rutile TiO_2(110). RSC Advances, 4(17), 8550-8557.

Levchenko, A.A., Li, G., Boerio-Goates, J., Woodfield, B.F., and Navrotsky, A. (2006) TiO_2 stability landscape: polymorphism, surface energy, and bound water energetics. Chemistry of Materials, 18(26), 6324-6332.

Li, C., Koenigsmann, C., Ding, W., Rudshteyn, B., Yang, K.R., Regan, K.P., Konezny, S.J., Batista, V.S., Brudvig, G.W., Schmuttenmaer, C.A., and Kim, J.-H. (2015) Facet-dependent photoelectrochemical performance of TiO_2 nanostructures: an experimental and computational study. Journal of the American Chemical Society, 137(4), 1520-1529.

Li, G., Li, L., Boerio-Goates, J., and Woodfield, B.F. (2003) Grain-growth kinetics of rutile TiO_2 nanocrystals under hydrothermal conditions. Journal of Materials Research, 18(11), 2664-2669.

Mattos L. V., Jacobs G., Davis B. H., and Noronha F. B. (2012) Production of hydrogen from ethanol: review of reaction mechanism and catalyst deactivation, Chemical Reviews, **112**(7), 4094-123.

Muir, J.N., Choi, Y., and Idriss, H. (2012) Computational study of ethanol adsorption and reaction over rutile TiO_2 (110) surfaces. Physical Chemistry Chemical Physics, 14(34), 11910-11919.

Paramasivam, I., Jha, H., Liu, N., and Schmuki, P. (2012) A Review of photocatalysis using self-organized TiO_2 nanotubes and other ordered oxide nanostructures. Small, 8(20), 3073-3103.

Radha, S., and Navrotsky, A. (2014) Energetics of CO_2 adsorption on Mg–Al layered double hydroxides and related mixed metal oxides. The Journal of Physical Chemistry C, 118(51), 29836-29844.

Rufner, J., Anderson, D., Benthem, K., and Castro R. (2013) Synthesis and sintering behavior of ultrafine (<10 nm) magnesium aluminate spinel nanoparticles. Journal of the American Ceramic Society, 96(7), 2077-2085.

Sanz-Pérez, E.S., Murdock, C.R., Didas, S.A., and Jones, C.W. (2016) Direct capture of CO_2 from ambient air. Chemical Reviews, 116(19), 11840-11876.

Scherrer, P. (1918) Bestimmung der Größe und der inneren Struktur von Kolloidteilchen mittels Röntgenstrahlen. Nachrichten von der Gesellschaft der Wissenschaften zu Göttingen, Mathematisch-Physikalische Klasse, 26, 98-100.

Schindler M. and Hochella M. F. (2015) Soil memory in mineral surface coatings: Environmental processes recorded at the nanoscale, Geology, **43**(5), 415-18.

Sclafani, A., and Herrmann, J.M. (1996) Comparison of the photoelectronic and photocatalytic activities of various anatase and rutile forms of titania in pure liquid organic phases and in aqueous solutions. The Journal of Physical Chemistry, 100(32), 13655-13661.

Silaghi, M.-C., Comas-Vives, A., and Copéret, C. (2016) CO_2 activation on Ni/γ–Al_2O_3 catalysts by first-principles calculations: from ideal surfaces to supported nanoparticles. ACS Catalysis, 6(7), 4501-4505.

Stangeland, K., Kalai, D., Li, H., and Yu, Z. (2017) CO_2 Methanation: the effect of catalysts and reaction conditions. Energy Procedia, 105, 2022-2027.

Strambeanu N., Demetrovici L., and Dragos D., Natural sources of nanoparticles, pp. 9-19. in Nanoparticles' Promises and Risks: Characterization, Manipulation, and Potential Hazards to Humanity and the Environment. Edited by M. Lungu, Neculae A., Bunoiu M., and Biris C. Springer International Publishing, Cham, 2015.

Sumita, M., Hu, C., and Tateyama, Y. (2010) Interface water on TiO_2 anatase (101) and (001) surfaces: first-principles study with TiO_2 slabs dipped in bulk water. The Journal of Physical Chemistry C, 114(43), 18529-18537.

Ushakov, S.V., and Navrotsky, A. (2005) Direct measurements of water adsorption enthalpy on hafnia and zirconia. Applied Physics Letters, 87(16), 164103.

Williamson, G.K., and Hall, W.H. (1953) X-ray line broadening from filed aluminium and wolfram. Acta Metallurgica, 1(1), 22-

Wu, D., and Navrotsky, A. (2013) Small molecule – silica interactions in porous silica structures. Geochimica et Cosmochimica Acta, 109, 38-50.

Wu, D., and Navrotsky, A. (2015) Probing the energetics of organic–nanoparticle interactions of ethanol on calcite. Proceedings of the National Academy of Sciences, 112(17), 5314-5318.

Wu, D., Guo, X., Sun, H., and Navrotsky, A. (2015) Energy landscape of water and ethanol on silica surfaces. The Journal of Physical Chemistry C, 119(27), 15428-15433.

Wu, D., Gassensmith, J.J., Gouvêa, D., Ushakov, S., Stoddart, J.F., and Navrotsky, A. (2013) Direct calorimetric measurement of enthalpy of adsorption of carbon dioxide on CD-MOF-2, a green metal–organic framework. Journal of the American Chemical Society, 135(18), 6790-6793.

Wu, Y.J., Li, P., Yu, J.G., Cunha, A.F., and Rodrigues, A.E. (2013) K-promoted hydrotalcites for CO_2 capture in sorption enhanced reactions. Chemical Engineering & Technology, 36(4), 567-574.

Xu, M., Gao, Y., Moreno, E.M., Kunst, M., Muhler, M., Wang, Y., Idriss, H., and Wöll, C. (2011) Photocatalytic activity of bulk TiO_2 anatase and rutile single crystals using infrared absorption spectroscopy. Physical Review Letters, 106(13), 138302.

Yahya, E. A., Zabidi, N. A. M., and Kait, C.F. (2016) A study on coke deposition in Ni-based catalysts for CO_2 reforming of methane. AIP Conference Proceedings, 1787(1), 030005.

Zhang, R., Liu, Z., Ling, L., and Wang, B. (2015) The effect of anatase TiO_2 surface structure on the behavior of ethanol adsorption and its initial dissociation step: A DFT study. Applied Surface Science, 353, 150-157.

This is a preprint, the final version is subject to change, of the American Mineralogist (MSA)
Cite as Authors (Year) Title. American Mineralogist, in press.
DOI: https://doi.org/10.2138/am-2019-6797

Table 1 Integral enthalpy (ΔH_{int}) of ethanol adsorption on oxide nanoparticles

Samples	SA	*Particle diameter*	Sample mass	Differential enthalpy of first dose	Surface coverage	Integral enthalpy	Amount of Ethanol adsorbed	
	(m^2/g)	*(nm)*	*(mg)*	*(kJ/mol)*	*($EtOH/nm^2$)*	*(kJ/mol of EtOH)*	*(mmol)*	*(mmol/g)*
Anatase								
1st run	256.65	7.1	25.3	-97.71	2.81	-77.14	0.0303	1.1989
2nd run			25.3	-82.00	0.64	-64.80	0.0069	0.2712
Rutile ***1st run***	80.49	29.8	45.94	-107.28	1.73	-100.57	0.0106	0.2319
2nd run			45.94	-109.05	0.47	-87.76	0.0029	0.0629
3rd run			45.94	-100.47	0.49	-83.70	0.0030	0.0653
γ-Al_2O_3								
1st run	86.78	19.7	22.28	-84.81	3.05	-72.46	0.0098	0.4400
2nd run			22.28	-88.50	1.20	-74.95	0.0038	0.1724
3rd run			22.28	-88.24	1.55	-68.99	0.0050	0.2228

Table 2 CO_2 adsorption of nano size TiO_2 and γ-Al_2O_3

sample	SA(m^2/g)	Particle diameter (nm)	Sample mass (mg)	Differential enthalpy for first dose (kJ/mol)	Surface coverage (CO_2/nm^2)	Integral enthalpy (kJ/mol CO_2)	Amount of CO_2 adsorbed (mmol/g)	Integral enthalpy (J/m^2)
TiO_2(Anatase)	256.65	7.1	28.57	-59.44	2.22	-41.58	0.9482	-0.1188
TiO_2(rutile)	80.49	29.8	38.16	-47.36	1.19	-39.09	0.1846	-0.0745
γ-Al_2O_3	86.78	19.7	14.7	-47.14	1.92	-33.69	0.2773	-0.1077

This is a preprint, the final version is subject to change, of the American Mineralogist (MSA)
Cite as Authors (Year) Title. American Mineralogist, in press.
DOI: https://doi.org/10.2138/am-2019-6797

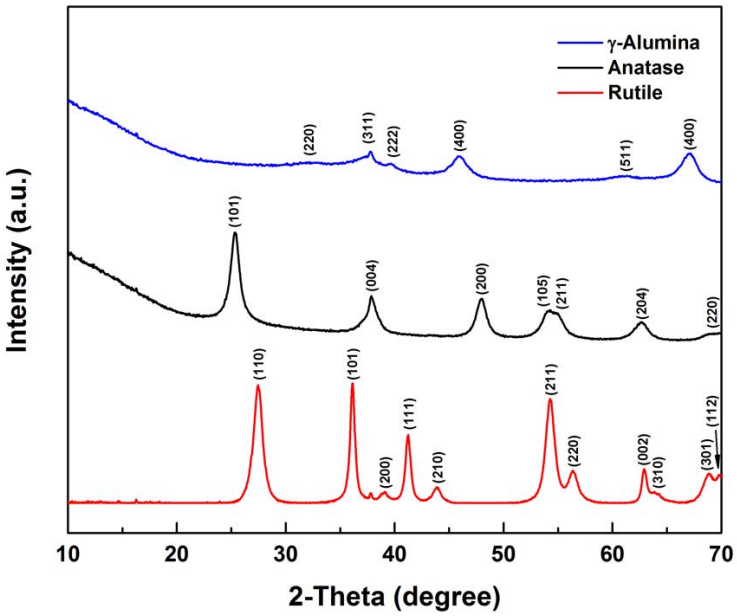

Figure 1 XRD patterns of nano-sized anatase, rutile TiO_2 and γ-alumina

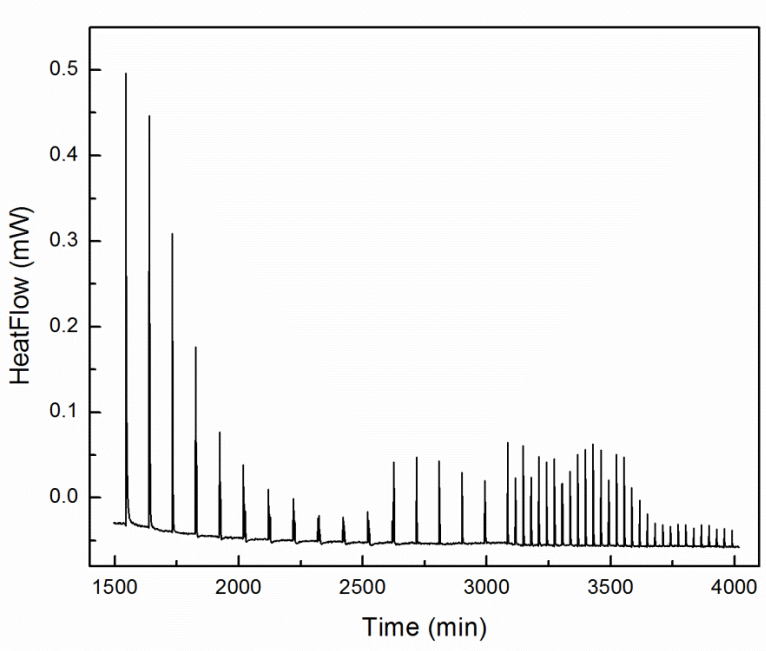

Figure 2 Typical heat signals from calorimetry for ethanol adsorption, example of first run on rutile.

This is a preprint, the final version is subject to change, of the American Mineralogist (MSA)
Cite as Authors (Year) Title. American Mineralogist, in press.
DOI: https://doi.org/10.2138/am-2019-6797

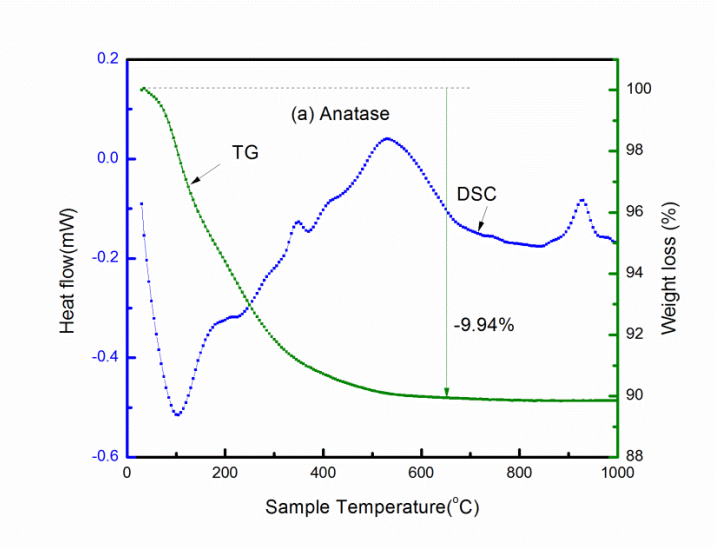

'5

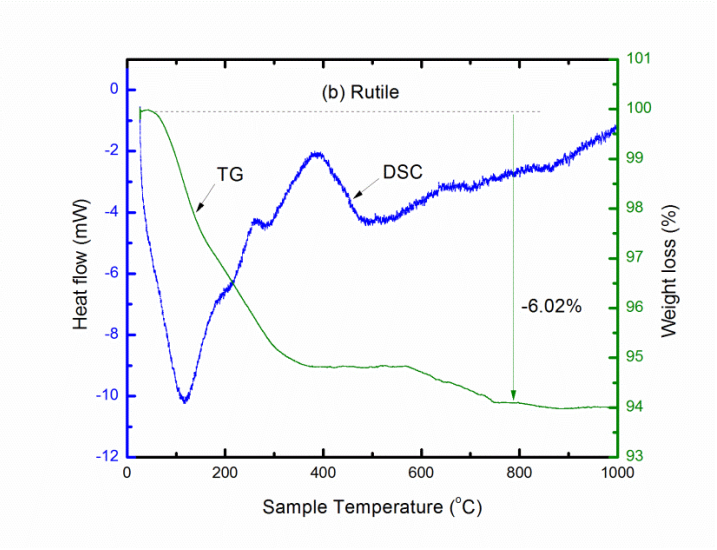

'6

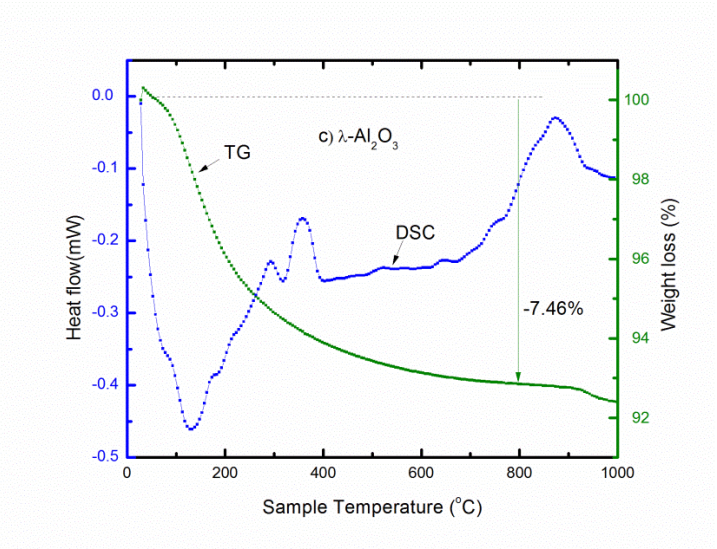

'7

'8 **Figure 3** DSC-TG curves of anatase(a) and rutile(b) TiO_2 and γ-Al_2O_3(c)

This is a preprint, the final version is subject to change, of the American Mineralogist (MSA)
Cite as Authors (Year) Title. American Mineralogist, in press.
DOI: https://doi.org/10.2138/am-2019-6797

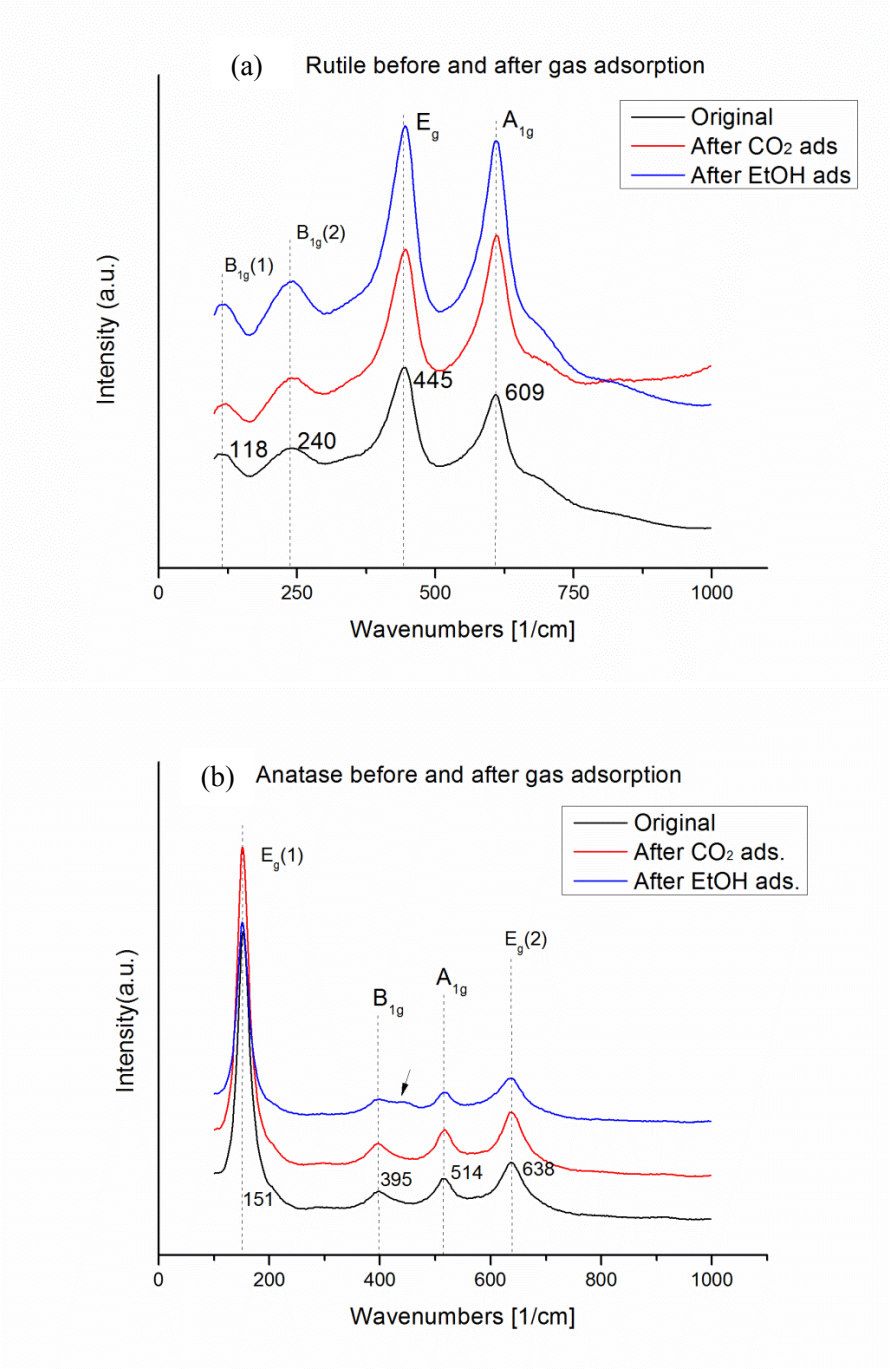

Figure 4 Raman spectra of (a) anatase TiO_2 and (b) rutile TiO_2 with and without gas adsorption

This is a preprint, the final version is subject to change, of the American Mineralogist (MSA)
Cite as Authors (Year) Title. American Mineralogist, in press.
DOI: https://doi.org/10.2138/am-2019-6797

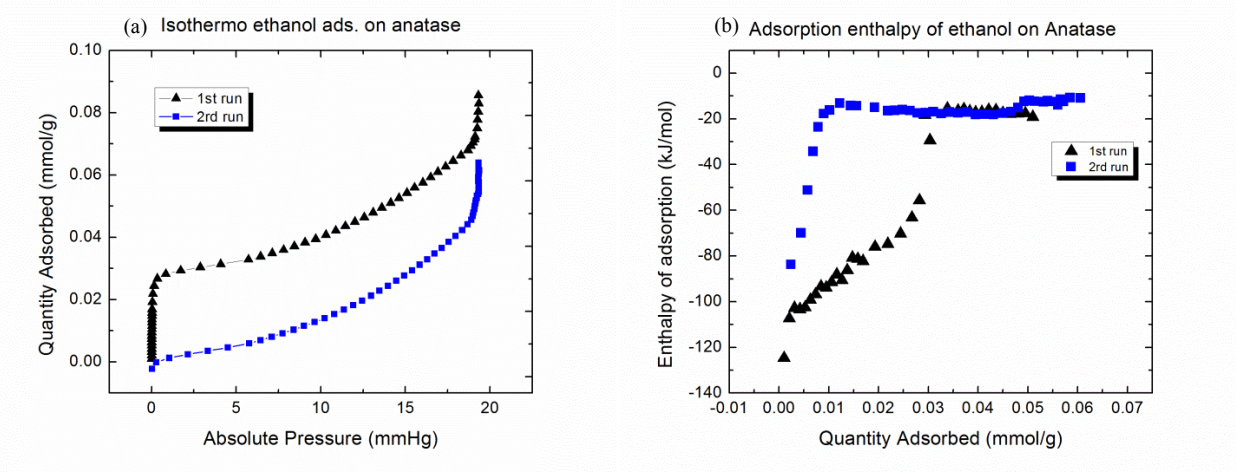

Figure 5 (a) Isotherm and (b) differential enthalpy of ethanol adsorption on anatase TiO_2

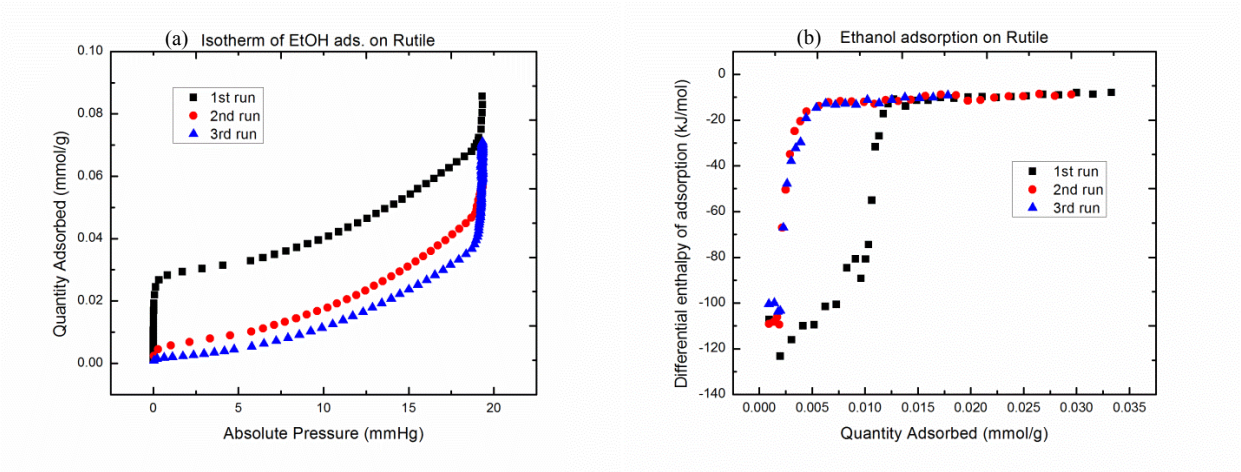

Figure 6 (a) Isotherm and (b) differential enthalpy of ethanol adsorption on rutile TiO_2

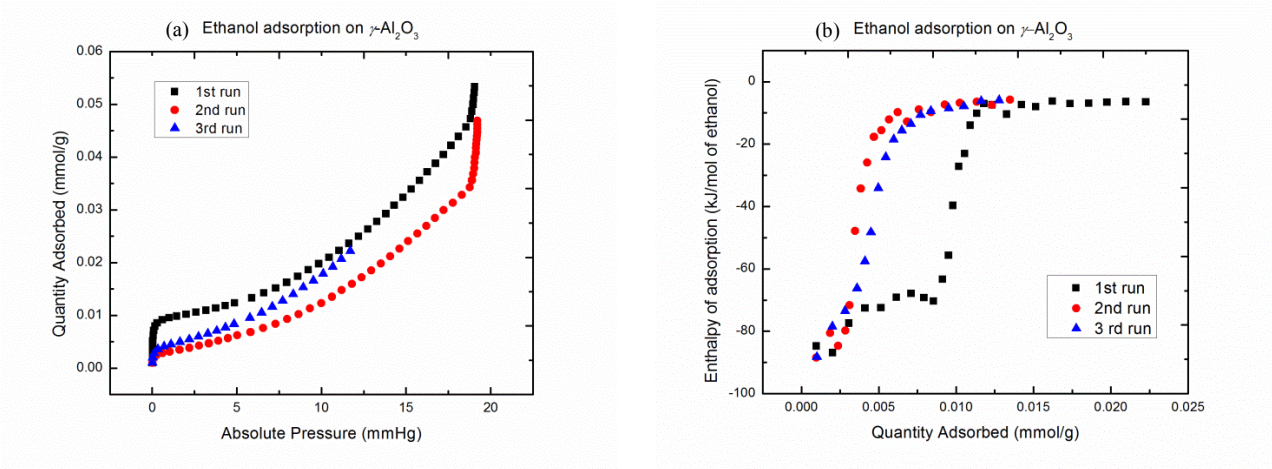

Figure 7 (a) Isotherm and (b) differential enthalpy of ethanol adsorption on γ-Al_2O_3

This is a preprint, the final version is subject to change, of the American Mineralogist (MSA)
Cite as Authors (Year) Title. American Mineralogist, in press.
DOI: https://doi.org/10.2138/am-2019-6797

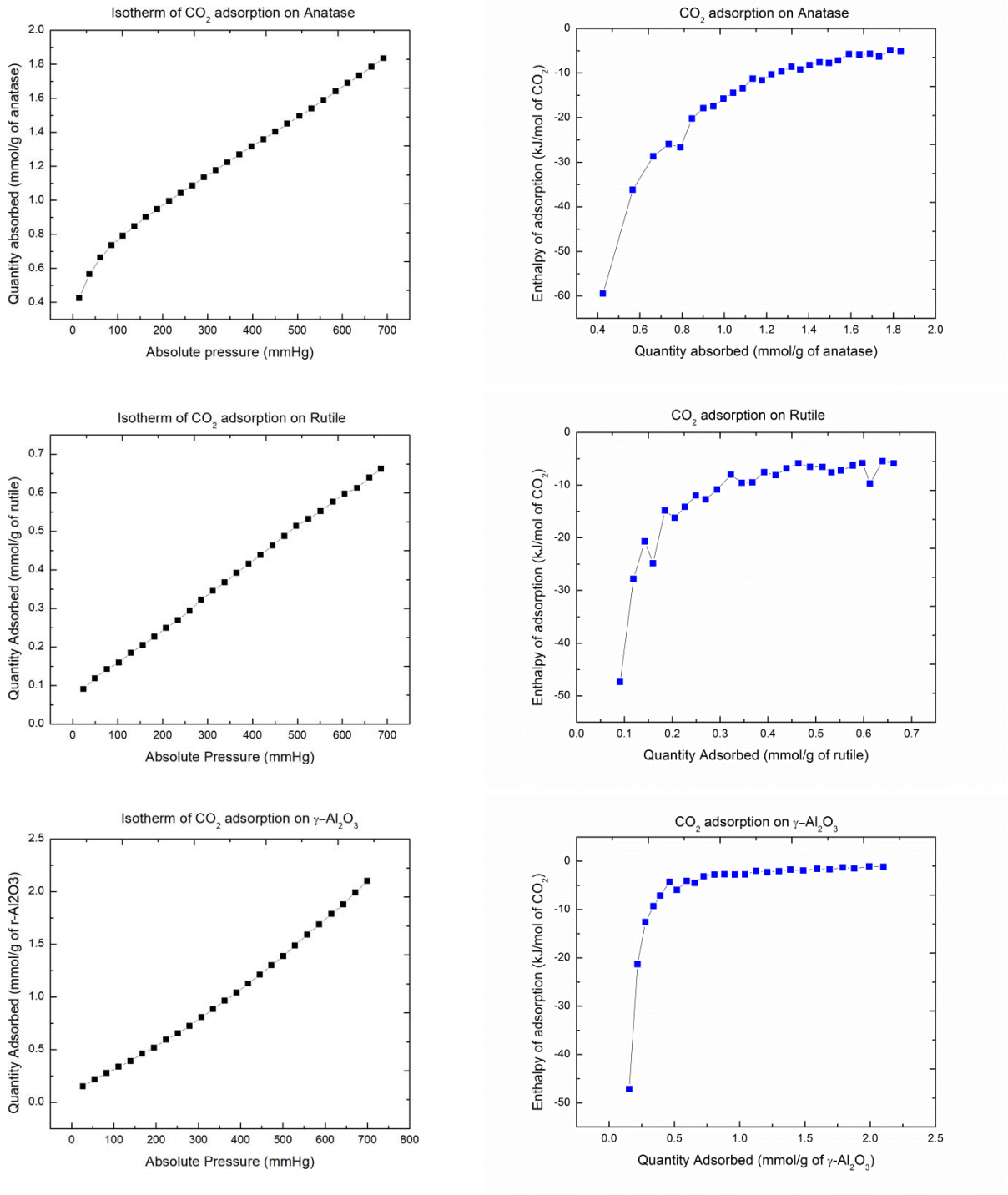

Figure 8 Isotherm and differential enthalpy of CO_2 adsorption on anatase, rutile and γ-Al_2O_3